Visible and near-ultraviolet absorption spectrum of ice from transmission of solar radiation into snow

Stephen G. Warren, Richard E. Brandt, and Thomas C. Grenfell

Snow is a scattering-dominated medium whose scattering is independent of wavelength at 350–600 nm. The attenuation of solar radiation in snow can be used to infer the spectral absorption coefficient of pure ice, by reference to a known value at 600 nm. The method is applied to clean Antarctic snow; the absorption minimum is at 390 nm, and the inferred absorption coefficient is lower than even the lowest values of the Antarctic Muon and Neutrino Detector Array (AMANDA) experiment on glacier ice: The absorption length is at least 700 m, by comparison with 240 m for AMANDA and 10 m from laboratory attenuation measurements.

OCIS codes: 160.4760, 010.2940, 290.4210.

1. Introduction

The spectral absorption coefficient of pure ice is needed to understand and predict the interaction of electromagnetic radiation with ice and ice-containing media such as snow and clouds. The general features of the spectrum are well known, for example, as reviewed by Warren.[1] Ice exhibits strong absorption in the ultraviolet (UV) at wavelengths $\lambda < 170$ nm. With increasing wavelength, the absorption becomes extremely weak in the visible, with a minimum near 400 nm. The absorption is moderate in the near infrared (IR), 1–3 μm, and strong through the IR, 3–150 μm, and then becomes weak again in the microwave region for $\lambda > 1$ cm. The absorption spectrum of liquid water generally parallels that of ice from the UV into the middle IR, but their spectra diverge for $\lambda > 10$ μm.

The visible and near-visible region lacks absorption mechanisms for ice, as it lies between the electronic absorptions of the UV and the vibrational absorptions of the IR. We will show that the absorption coefficient k_{ice} is probably less than 0.1 m^{-1} for nearly the entire domain of 300–600 nm. The reciprocal of k_{ice} is the absorption length, the mean free path of photons before absorption; ${k_{\text{ice}}}^{-1}$ exceeds 10 m for this spectral region, which includes the peak of the solar energy spectrum.

Between 300 and 600 nm the absorption by ice is so weak that for some geophysical purposes it may as well be set to zero, for example, when computing absorption of solar radiation by ice clouds, because path lengths of photons through atmospheric ice crystals are very small compared to the absorption length. Clean fine-grained snow reflects 97–99% of the incident sunlight in this spectral region,[2] and the error bars sometimes encompass 100% reflectance, again consistent with a near-zero absorption coefficient.

In media with minimal scattering, however, accurate values of the absorption coefficient are needed even where it is extremely small. This is true for ocean water and for glacier ice, where significant absorption of sunlight can occur at depths of many meters. For example, the predicted equilibrium ice thickness on the tropical ocean of "Snowball" Earth is sensitive to the exact value of k_{ice} at visible wavelengths.[3]

2. Prior Measurements

Sauberer[4] cut blocks of ice of length 15–50 cm from a lake in Austria and measured their transmission of radiation for wavelengths of 313–800 nm. These blocks were too short to accurately quantify the absorption at its minimum near 400 nm; even his longest block attenuated the beam by only 2%. He also measured near-IR transmission through 7-mm samples at wavelengths of 800–1300 nm, but with less accuracy.

The authors are with the Department of Atmospheric Sciences, University of Washington, Seattle, Washington 98195. The e-mail address for S. G. Warren is sgw@atmos.washington.edu.

Received 23 November 2005; revised 14 February 2006; accepted 14 February 2006; posted 9 March 2006 (Doc. ID 66188).

0003-6935/06/215320-15$15.00/0

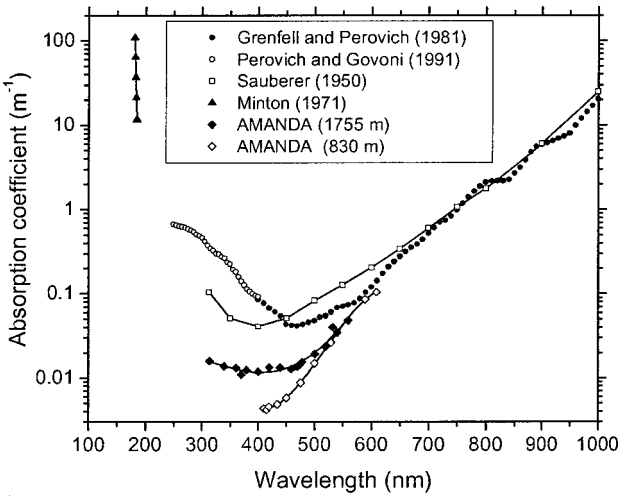

Fig. 1. Prior reported values of the spectral absorption coefficient of pure ice from Sauberer,[4] Grenfell and Perovich,[5] Perovich and Govoni,[6] and the AMANDA project.[7–11] The two sets of AMANDA values are for ice at different depths, as indicated. The values from Minton[12] plotted here are a factor of 2.3 higher than in Warren's review.[1] Minton's reported extinction coefficients were defined on base-10 (Refs. 13 and 14) but were misinterpreted in Warren's review[1] as extinction coefficients on base-e.[15]

Sauberer's measurements (Fig. 1) were used for 30 years until they were superseded by those of Grenfell and Perovich[5] (hereinafter GP). GP grew a block of ice 2.8 m long from a tank of filtered deionized water; the ice was grown from the bottom up to prevent incorporation of bubbles. The ice was polycrystalline, but scattering from the crystal boundaries appeared to be negligible, so the attenuation was interpreted as entirely due to absorption, after accounting for Fresnel reflection at the two ends. GP's measurements on this block of ice (and on shorter blocks for longer wavelengths) agreed with those of Sauberer for 700–1000 nm (Fig. 1). Between 400 and 700 nm they were shifted in wavelength, with Sauberer's minimum at 400 nm but GP's at 470 nm. Their values of minimum absorption were in close agreement, $k_{\mathrm{ice}} = 0.04\ \mathrm{m}^{-1}$, which is somewhat surprising since Sauberer's ice was unpurified lake ice. However, the process of freezing can cause rejection of impurities if the freezing rate is slow enough.

Ten years later, Perovich and Govoni[6] (hereinafter PG) used the same method as GP with a 3 m long sample to extend the GP measurements into the UV, 250–400 nm. They found a steady decrease of k_{ice} from $0.7\ \mathrm{m}^{-1}$ at 250 nm to $0.08\ \mathrm{m}^{-1}$ at 400 nm, where their measurements agreed with GP's value at that wavelength (Fig. 1).

Sauberer, GP, and PG attributed their measured attenuation to absorption alone. If a small amount of undetectable scattering was present, the reported absorption coefficient would be too large. Recently, coefficients for both absorption and scattering have been inferred for subsurface ice 800–1800 m deep in the Antarctic ice sheet at the South Pole. What is measured is the distribution of photon arrival times at an array of detectors embedded in the ice, the photons originating from a pulsed source.[7–11] Those measurements were made to determine the clarity of ice at various depths for the Antarctic Muon and Neutrino Detector Array (AMANDA). At these depths the scattering coefficient is small because most of the air has dissolved in the ice as clathrates, so there are few bubbles.

The AMANDA absorption coefficients (Fig. 1) agree with the laboratory measurements at $\lambda = 600$ nm, but at shorter wavelengths AMANDA infers a smaller k_{ice} than obtained in the laboratory, suggesting that the laboratory ice did indeed scatter a small amount of light; this scattering could have dominated the attenuation at blue wavelengths because the absorption is so weak there. The laboratory measurements were made at higher temperatures than the South Polar ice, but the temperature dependence of k_{ice} (1%/deg)[16] is much too weak to explain the discrepancy.

The AMANDA results imply that the absorption of pure ice reaches a minimum in the near UV, 350–400 nm. However, the absorption by ice is so weak in the visible and UV that absorption in Antarctic ice is dominated by the small amount of dust naturally present in the ice. The absorption is stronger in ice that fell as snow during the last ice age,[17] when the snow accumulation rate was lower and the atmosphere was dustier. The lower curve of AMANDA results shown in Fig. 1 is for the cleanest ice in the bubble-free region. The AMANDA workers infer that the true absorption coefficient of pure ice is even lower than the lowest values measured.

The wavelength dependence of the attenuation measured by PG and GP for 200–470 nm is indeed what would be expected if Rayleigh scattering is dominant: Figure 5 of Ref. 9 shows that the reported absorption coefficient in this spectral region is proportional to λ^{-4}, not only for ice but also for LiF, $BaTiO_3$, and diamond. The scattering would be caused by crystal defects with dimensions much smaller than the wavelength of light.

On the other hand, there is much field evidence favoring the GP–PG spectrum over the AMANDA spectrum, in that the spectral albedos (reflectances) of snow, sea ice, glacier ice, and icebergs peak at $\lambda \approx 470$ nm, as is expected if the absorption coefficient reaches a minimum at that wavelength. Some of these albedos are shown in Fig. 2. Snow spectral albedo was measured at the South Pole[2] and in northern Japan.[19] Cold glacier ice was measured near Mount Howe in the Transantarctic Mountains.[3,20] Bare cold sea ice was measured at the coast of Antarctica.[21] Marine ice is clear ice that forms by the freezing of seawater to the base of ice shelves; it is highly desalinated, unlike sea ice freezing at the ocean surface.[23] It can be exposed to view if the iceberg capsizes, and its spectral albedo has been measured.[22] Various forms of Arctic sea ice, bare or snow covered, gave peak albedos near 500 nm.[24] Snow-

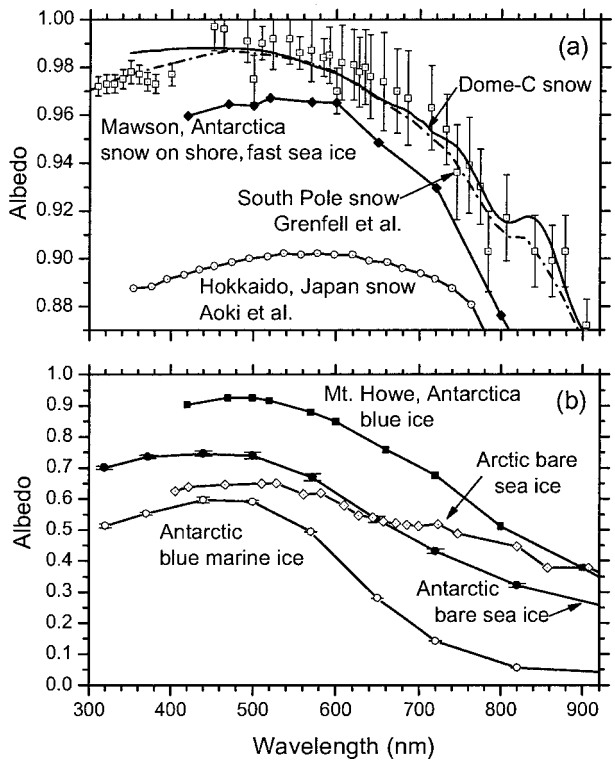

Fig. 2. Spectral albedo measurements for natural snow and ice surfaces. (a) Snow at the South Pole[2] and at Dome C, snow-covered sea ice at the coast of Antarctica,[18] and snow in Japan.[19] The curve through the South Pole measurements is the result of a radiative transfer model that used the laboratory measurements of k_{ice} (Fig. 4 of Ref. 2). (b) Cold glacier ice at Mount Howe in the Transantarctic Mountains,[3,20] bare cold thick sea ice at the coast of Antarctica,[21] blue marine ice of an iceberg,[22] and bare Arctic sea ice (from Fig. 2 of Ref. 24). Note that the vertical axis in (a) differs from that in (b).

covered Antarctic sea ice has also been measured; it likewise exhibits a peak at 450–500 nm.[18,21]

However, in each of these cases an explanation can be found that would allow the peak albedo to be shifted from the wavelength of minimum ice absorption to longer wavelengths, so that the albedo measurements may all be consistent with the AMANDA spectrum for pure ice. In most cases this is because the likely impurities (organic matter or soil dust) have absorption spectra that generally decrease with wavelength from 300 to 600 nm, accounting for their red, brown, and yellow colors.[23,25] Bare sea ice contains brine pockets that are home to algae. The snow cover on sea ice is also not pristine, as penguins and seals travel across it and, in fact, were nearby when the Antarctic sea ice measurements in Fig. 2 were made. Our measurements on blue ice at Mount Howe[20] show a peak of albedo between 430 and 500 nm as expected for GP's ice absorption spectrum, but the proximity of this ice to the rock dust on Mount Howe raises the possibility of impure ice at that location. Our measurements of the blue marine ice of an iceberg also showed a peak albedo between 430 and 500 nm, but in this case there is the possibility of dissolved organic matter from the seawater causing absorption of UV and blue light.[23] The Antarctic ice surfaces in Fig. 7(b) were measured under clear sky with low Sun. Since the ice albedo increases with increasing incidence angle, the fact that the diffuse fraction of sunlight increases as wavelength decreases may also contribute to the decrease of albedo from 470 to 300 nm.

We are left with the snow albedo spectra. The snow in Hokkaido measured by Aoki *et al.*[19] contained some soil dust, which shifted the peak albedo to near 700 nm in most of their measurements. The plot selected for display in Fig. 2(a) here is the one having the shortest peak wavelength. Gerland *et al.*[26] did find albedo to peak at $\lambda < 400$ nm in Svalbard in May, but the peak shifted to ~530 nm in June as dust became significant.

Dust and organic matter cannot explain the spectral peak of snow albedo at the South Pole [top plot in Fig. 2(a)]. Those measurements were made 500 m upwind of the station, where the content of absorptive impurities [<0.5 parts per billion (ppb) of black carbon][27] is too small to affect the albedo measurably (although this low impurity level can affect transmission measurements as shown below). The South Pole albedo plot shows a broad peak in the region of $\lambda = 470$ nm as is predicted from radiative transfer modeling if the absorption coefficient of ice reaches a minimum at that wavelength. The albedo is so high here that the measurements cannot locate the peak precisely, but the significantly lower albedos in the near UV do indicate the wavelength of minimum absorption to be at $\lambda > 400$ nm. However, for South Polar snow the UV and visible measurements were made with different instruments. The two instruments were of different sizes and had different support legs, so they shadowed the snow surface by different amounts. We estimated the shadowing correction as 1% for the visible–IR radiometer and 0.5% for the UV radiometer. Any error in the estimated shadowing corrections could therefore cause the UV albedos to be offset slightly from the visible albedos, as they do appear to be in Fig. 2(a). Support for this explanation comes from the spectral albedo of Antarctic snow measured at Dome C in conjunction with the experiment reported in this paper; it is indicated in Fig. 2(a). That spectrum was measured with a single instrument, so the shadowing factor is constant. The albedo is high and flat from 350 to 500 nm, unlike the other measurements in Fig. 2.

We conclude that, although most measurements of spectral albedo show peaks at $\lambda > 450$ nm, they cannot rule out an absorption minimum for pure ice at $\lambda \leq 400$ nm. Another piece of evidence favoring the laboratory measurements is that PG[6] obtained nearly the same value of attenuation coefficient at $\lambda = 400$ nm as GP[5] on different blocks of ice grown ten years apart. This result argues for attenuation being dominated by absorption, since the scattering would be expected to depend on crystal sizes and therefore on the temperature gradient through the ice during growth. However, the same procedure for ice growth

was used in the two experiments, and the growth rate of ice was approximately the same, so the scattering could also be the same.

The purpose of this paper is to address the discrepancy between the laboratory measurements and the AMANDA measurements by providing evidence from an independent experiment.

3. Snow Transmission Experiment

The AMANDA experiment discussed above obtained an absorption spectrum $k_{ice}(\lambda)$ by an indirect method. Here we develop another indirect method to infer $k_{ice}(\lambda)$, which is quite different from both the laboratory experiment and the AMANDA experiment. In the laboratory experiments of GP and PG, attenuation was measured in a medium whose scattering was very weak, but whose scattering coefficient was strongly wavelength dependent, probably proportional to λ^{-4}. In the snow transmission method described here, we measure attenuation in a medium dominated by scattering, but whose scattering is nearly independent of wavelength.

In this paper, the terminology is as follows. The absorption coefficient of pure ice is k_{ice}. Snow has a radiance extinction coefficient, which is the sum of its scattering and absorption coefficients:

$$\sigma_{ext} = \sigma_{scat} + \sigma_{abs}. \quad (1)$$

The quantities in Eq. (1) are the inherent optical properties that are input to radiative transfer theory. What is obtained directly from transmission measurements in snow is a flux extinction coefficient k_{ext}, which includes the effects of multiple scattering in a snowpack. It is related (in Section 4) to the radiance extinction coefficient by radiative transfer theory. All five quantities have units of inverse length (m^{-1}). For snow, the measured density is used to convert from geometric depth to ice-equivalent depth (the density of ice is 917 kg m^{-3}; the density of the sampled snow was 300–400 kg m^{-3}).

As Fig. 2 shows, the wavelength dependence of snow albedo is very weak; the albedo is near 100% from 300 to 600 nm, so albedo measurements, within their uncertainty, are not useful to obtain quantitative values of the spectral absorption coefficient. In transmission, however, the different wavelengths have quite different attenuation lengths. This contrast between albedo and transmission can easily be seen by poking a hole into snow with an ice axe; the snow surface appears white but the light emerging from the bottom of the hole is deep blue.[28]

A. Experimental Design

A first trial of the method was carried out at the French–Italian Antarctic station at Dome C (75°S, 123°E, 3230 m) in December 2004 to January 2005. At this location the snow accumulates slowly throughout the year and never melts; summer temperatures are always far below freezing, even at midday. Most of the measurements were made 2 km west of the station, in the vicinity of a tower that was built for measuring bidirectional reflectance of snow. Some of the measurements were made 3 km southwest of the station, inside the Special Protected Area (from which vehicles are always excluded).

We used a scanning portable spectroradiometer manufactured by Analytical Spectral Devices (ASD). The instrument employs three separate grating spectrometers that simultaneously measure radiance across three wavelength regions covering 350–2500 nm; for this experiment we used data only from the first grating, covering the range of 350–1000 nm. The spectral resolution is 3 nm in this band. The instrument can average 100 scans in 10 s. It is designed specifically to cover the solar spectrum and has order-blocking and cutoff filters to ensure uncontaminated spectra. The spectroradiometer and its computer, both battery powered, were housed in separate insulated boxes with clear windows; they were mounted on a sled that was pulled by manpower to locations distant from buildings and vehicles. At ambient temperatures of −20° to −30 °C the electronics were kept warm enough to operate for ~1 hour by self-heating supplemented by bottles of hot water.

A fiber-optics guide, which feeds light into the spectroradiometer, was mounted in a hollow rod that was inserted vertically into the undisturbed snow. At depths greater than a few centimeters, the radiation field is diffuse, varying little with direction. Measurements were made observing in the vertical direction, sampling the upwelling diffuse radiation. (A horizontal view was used in preliminary measurements during the previous year, which gave results qualitatively in agreement with those of the vertical view.) This method of measuring transmission of diffuse radiation is preferable to the traditional method of inserting a probe horizontally into the wall of a snow pit, because the open pit significantly alters the radiation field.

Transmission measurements were carried out on cloudless days in late December and early January, near local noon, so that the incident solar radiation flux would be high and constant during each series of measurements. The probe was inserted into snow on the sunward (north) side of the sled, 50–60 cm distant from the sled. Spectral scans were recorded at approximately 5 cm intervals down to 135 cm. The procedure was repeated at several nearby sites until the instrument box became too cold. Then a pit was dug for measurement of density and photography of snow grains every 5 cm. Radiation measurements in the topmost snow layers (approximately the top 40 cm) are not used in the analysis here, for several reasons. (1) Variation of snow grain size with depth is most rapid in the topmost few centimeters.[29] (2) Near the surface, radiation flux is not attenuated exponentially with depth. However, at sufficient optical depth below the surface, in a uniform medium that both absorbs and scatters light, both the downward flux and the upward flux are attenuated exponentially (in snow, 1 cm is usually sufficient to reach the exponential regime). (3) Construction of the tower during January 2003 caused contamination of the upper

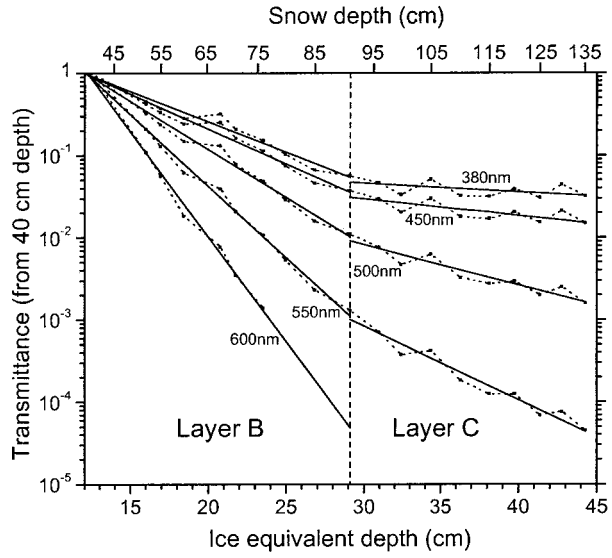

Fig. 3. Transmission of solar radiation flux into snow at selected wavelengths, relative to the flux measured at a reference depth of 40 cm [Eq. (2)], at Dome C, Antarctica, 5 January 2005, near local noon, 2 km west of the station and 200 m north of the walk-up tower. Linear fits are shown for two depth ranges: 40–90 cm (layer B) and 90–135 cm (layer C). Snow depths (top horizontal scale) have been converted to ice-equivalent depths (bottom scale) using the measured density profile, which varied in the range of 300–400 kg/m^3.

snow at some of our sites; the 2003 layer was at 20 cm depth during our measurements two years later. We therefore use a reference depth z_0 somewhere between 30 and 40 cm snow depth (or 9–13 cm liquid-equivalent depth) and define the transmittance t into deeper snow as

$$t_\lambda(z_0, z) = \frac{I_\lambda(z)}{I_\lambda(z_0)}, \tag{2}$$

where I is the radiance received within the fiber-optics' downward-looking field of view, which is ~25 deg.

B. Experimental Results

In the exponential regime, the transmittance can be related to the asymptotic flux extinction coefficient k_{ext}:

$$t_\lambda(z_0, z) = \exp[-(z - z_0)k_{\text{ext}}(\lambda)]. \tag{3}$$

For monochromatic radiation, plots of $\log(t)$ versus z (in units of ice-equivalent depth) are approximately straight lines with slope $-k_{\text{ext}}$. Figure 3 shows these plots for several wavelengths for one of our experiments. Similar plots have been presented by Liljequist[30] and Grenfell and Maykut,[31] as reviewed by Warren.[32]

The increase of k_{ext} with increasing wavelength is apparent in Fig. 3. The data are fitted by least-squares lines. However, there is an apparent break in the slope at a snow depth of 90 cm, corresponding to a snow age of eight years. We therefore perform separate fits above and below 90 cm. (Because the point at 90 cm is as much subject to measurement error as any of the other subsurface points, we do not force the lines below 90 cm to pass through the value measured at 90 cm.) We define three layers: Layer A (0–40 cm) is the topmost snow, potentially contaminated during erection of the nearby tower in 2003; layer B (40–90 cm) is snow that fell between 1997 (the year the station was established) and 2002; and layer C (90–135 cm) contains snow that fell prior to 1997.

Possible reasons for the larger slopes in layer B are smaller snow grains and more impurities. Snow metamorphism causes individual snow crystals to merge, so the average grain size increases with time[33]; however, this process is slow at the low temperatures of the Antarctic Plateau. Black carbon (soot) is emitted by vehicles at the station and by the station's power plant. The prevailing wind direction is from the southwest, but winds can at times come from any direction, so our measurement sites 2 km west of the station are expected to contain some soot in the upper snow layers. We show below that the differences in k_{ext} between layer B and layer C are probably due to differences in grain size and to differences in soot content.

The deviations of the data from straight lines within each layer are partly due to grain-size variations within the layer; σ_{scat} is smaller for larger grains. However, the major reason is probably unresolved density variations causing an imperfect conversion of snow depth to ice-equivalent depth. Some of the experiments also probably suffered from a changing incident solar flux due to subvisible clouds. Of a total of 25 experiments, the one shown in Fig. 3 (5 January, hole 4) exhibited the smallest deviations from straight lines, and it was the only one in which the noise level in layer C was small enough for analysis. Below we will show that analysis of layer C is essential for separating the contributions of soot and ice in the absorption. We therefore focus our analysis on this one experiment.

The values of k_{ext} obtained from the slopes in Fig. 3 are plotted in Fig. 4, along with those of all other wavelengths from 350 to 600 nm, on both linear and logarithmic scales. No results are shown for $\lambda > 600$ nm because the absorption is so strong at these wavelengths that the radiance drops below the detection limit a short distance below z_0.

For layer C, experimental values of k_{ext} are shown only for 350–550 nm; radiation at wavelengths of 550–600 nm does not extend far enough into layer C for inference of k_{ext}. In Fig. 4, the point plotted for layer C at 600 nm will be explained later; it is our prediction of k_{ext} from the analysis in Appendix A. In Fig. 4 we have joined this point to the experimental points by a curve that approximately fits the measured data for 500–550 nm.

For visible and near-UV radiation, $\sigma_{\text{scat}} \gg \sigma_{\text{abs}}$, and the scattering efficiency of snow grains is nearly independent of wavelength (Fig. 2 of Wiscombe and Warren,[34] hereinafter WW). Therefore the maximum albedo and the minimum k_{ext} should both be found at

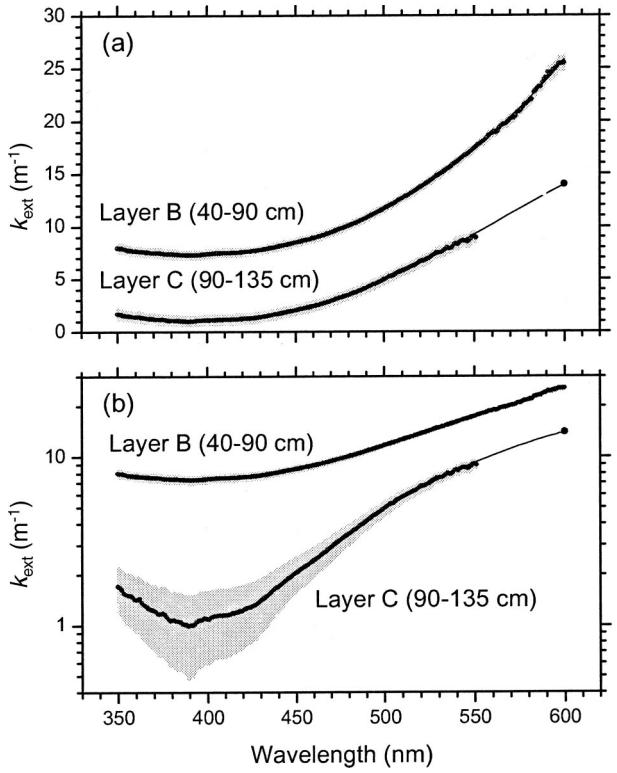

Fig. 4. Flux extinction coefficients for snow at Dome C on 5 January 2005 for two layers. These values were obtained from the slopes in Fig. 3. The units of k_{ext} are per meter of ice equivalent. (a) Linear scale. (b) Logarithmic scale. The measured data for layer C terminate at 550 nm; the point at 600 nm and the curve joining this point to the measured values involve a determination of the ratio of snow grain sizes for layers B and C, as explained in the text. The uncertainty in the slopes of linear fits in Fig. 3 is shown as the shaded band around each plot (1 standard deviation).

the wavelength of minimum absorption (λ_{min}). Figure 4 indicates that σ_{abs} reaches its minimum at 390 nm in both layers B and C. This same minimum was found at all locations, both near the tower and in the Special Protected Area, indicating that varying amounts of soot pollution from station activities are not sufficient to move λ_{min}. The same value of λ_{min} was found the previous year at Dome C in preliminary experiments using a different optical fiber with different viewing geometry and two different radiometers. We also tried different positions of the sled relative to the probe, but always obtained the same value of λ_{min}. The snow transmission experiment therefore finds λ_{min} to agree with that of AMANDA rather than that of the laboratory measurements. In Section 4 we use the snow transmission measurements to estimate quantitative values of k_{ice}; they will turn out to be lower than the lowest AMANDA values.

C. Comparison with Prior Measurements of Snow Spectral Transmittance

There have been several prior reports of snow spectral transmittance. Various experimental designs were used; many of them disturbed the snow significantly. In some published measurements the wavelength of minimum k_{ext} was found at $\lambda > 390$ nm, suggesting that blue-absorbing impurities contributed to the absorption, as we speculated above for the albedo measurements. Beaglehole *et al.*[35] found λ_{min} between 400 and 550 nm on Ross Island, Antarctica, where dust from a nearby volcano could have affected the measurements. They reported visible dust in their snow samples. Bourgeois,[36] as quoted by Raschke and Ohmura,[37] found $\lambda_{min} = 470$ nm in Alpine snow, where contamination by Saharan dust often occurs.[38] At Alert on Ellesmere Island (Canada), King and Simpson[39] found a weak dependence of k_{ext} on λ, with $\lambda_{min} \approx 500$ nm in an artificial snowpack. They suspected contamination by organic matter and soils because of the proximity of bare ground.

In Antarctic snow, Liljequist[30] measured transmittance, but his filters were too broad to resolve the transmission spectrally. However, the smallest k_{ext} was found in his blue filter, suggesting that $\lambda_{min} < 430$ nm. Kuhn and Siogas[40] found $\lambda_{min} = 500$ nm at the South Pole, but with considerable uncertainty because the procedure involved significant disturbance of the snow.[41]

Because of the improved experimental design and the low levels of contamination in the Dome C snow, our measurements of k_{ext} should be more suitable for analysis of ice absorption than any of the previous measurements.

4. Deriving Ice Absorption Coefficients from Snow Extinction Coefficients

A. Theory for Pure Snow

We will derive a method to obtain quantitative values of k_{ice} from snow transmission measurements, which requires that we have independent knowledge of k_{ice} at one of the wavelengths measured. This reference wavelength, λ_0, will be 600 nm, where AMANDA is in agreement with the laboratory measurements. The method derived in this Subsection, by assuming that all the absorption is due to ice, turns out to be extremely simple. Deriving k_{ice} in the presence of absorptive impurities (Appendix A) is more complex.

We first introduce some single-scattering quantities used in radiative transfer theory. (1) The extinction efficiency Q_{ext} is the (unitless) ratio of the extinction cross section of a particle to its geometric cross section. It is the sum of absorption and scattering efficiencies:

$$Q_{ext} = Q_{abs} + Q_{scat}. \tag{4}$$

(2) The single-scattering albedo $\bar{\omega}$ is the ratio of the radiance scattering coefficient to the radiance extinction coefficient:

$$\bar{\omega} \equiv \frac{\sigma_{scat}}{\sigma_{ext}} = \frac{\sigma_{scat}}{\sigma_{abs} + \sigma_{scat}}. \tag{5}$$

For a single particle,

$$\bar{\omega} = \frac{Q_{\text{scat}}}{Q_{\text{ext}}} = \frac{Q_{\text{scat}}}{Q_{\text{abs}} + Q_{\text{scat}}}. \quad (6)$$

(3) The single-scattering phase function describes the probability of scattering into a particular direction, when a photon encounters a particle (in this case, a snow grain). The first Legendre moment of the phase function is called the asymmetry factor g; it is the average value of the cosine of the scattering angle. From radiative transfer theory, the observed asymptotic (i.e., far from the boundaries) flux extinction coefficient k_{ext} is related to these single-scattering quantities by

$$k_{\text{ext}} = \sigma_{\text{ext}}\sqrt{(1-\bar{\omega})(1-\bar{\omega}g)}. \quad (7)$$

This is Eq. (7) of Ref. 42, derived from the Eddington approximation. The same equation results from the discrete ordinates method or the two-stream method (Eq. 26 of Ref. 43). Our procedure will be to use Eq. (7), together with the known value of k_{ice} at $\lambda_0 = 600$ nm, to infer k_{ice} at shorter wavelengths.

Our single-scattering calculations for snow grains use Mie theory,[44] which computes the interaction of radiation with ice spheres. We represent a nonspherical snow grain by an assembly of spheres having the same total surface area A and the same total volume V. The radius of the equivalent sphere is therefore determined by the requirement that the sphere has the same V/A ratio as the snow grain. This approach is justified by comparison of modeled with measured spectral albedo of snow[45] and by comparison of radiative fluxes in ice clouds computed exactly with those computed with the equivalent-sphere parameterization.[46–48] Although falling snow crystals are highly nonspherical, the grains of Antarctic surface snow are well rounded and nearly equidimensional because they have been broken and eroded by wind drifting.

For snow grains, the asymmetry factor is nearly constant across our wavelength domain of interest. For grain radii of 50–200 μm (typical of Antarctic snow in the top meter), $g = 0.885 \pm 0.002$ for wavelengths of 300–600 nm (Fig. 4 of WW). The single-scattering albedo $\bar{\omega}$ exceeds 0.9999 for these wavelengths (Fig. 3 of WW), so the quantity $(1 - \bar{\omega}g)$ in Eq. (7) is just $(1 - g)$, and it can be assumed independent of wavelength and grain size.

The extinction coefficient σ_{ext} is independent of wavelength but inversely proportional to grain size, as follows.

Let n_i be the number density of ice particles (particles per cubic meter). The ice particle effective radius is r_i (the subscripts will be needed in Appendix A where we must distinguish ice particles from soot particles). The extinction coefficient is related to the extinction efficiency by

Table 1. Dependences of Radiative Transfer Quantities within the Domains of 350–600 nm for Wavelength λ, 20–200 μm for Snow Grain Radius r_i, and 0–100 ppb for Soot Concentration C

	Dependent On		
Quantity	λ	r_i	C
σ_{ext}	No	Yes	No
σ_{abs}	Yes	No	Yes
$(1 - \bar{\omega})$	Yes	Yes	Yes
$(1 - \bar{\omega}g)$	No	No	No

$$\sigma_{\text{ext}}^{\text{ice}} = n_i \pi r_i^2 Q_{\text{ext}}^{\text{ice}}. \quad (8)$$

The snow density is the product of n_i and the mass of a snow grain:

$$\rho_{\text{snow}} = n_i \frac{4}{3} \pi r_i^3 \rho_{\text{ice}}. \quad (9)$$

Combining Eqs. (8) and (9), we obtain

$$\sigma_{\text{ext}}^{\text{ice}} = \frac{3}{4} \frac{Q_{\text{ext}}^{\text{ice}} \rho_{\text{snow}}}{r_i \rho_{\text{ice}}}. \quad (10)$$

However, since our snow depths are converted to ice-equivalent depths for analysis,

$$\sigma_{\text{ext}}^{\text{ice}} = \frac{3}{4} \frac{Q_{\text{ext}}^{\text{ice}}}{r_i}. \quad (11)$$

For particles with radius $r \gg \lambda$, $Q_{\text{ext}} \approx 2.0$. This approximation is accurate for the interaction of snow grains with visible and UV radiation. For example, for $r = 50$ μm, $Q_{\text{ext}}^{\text{ice}} = 2.025 \pm 0.004$ for wavelengths of 300–600 nm (Fig. 2 of WW). The average grain size in layer B (r_B) will differ from that in layer C (r_C), but within each layer the average grain size will be the same for all wavelengths. We therefore can assume $\sigma_{\text{ext}}^{\text{ice}}$ to be independent of λ in Eq. (7). Table 1 gives a summary of the dependence of the key radiative transfer quantities on wavelength, grain size, and soot content.

Now we compare measurements at two wavelengths, one of which is our reference wavelength $\lambda_0 = 600$ nm. From Eq. (7), with the approximations justified above (σ_{ext} and $1 - \bar{\omega}g$ both independent of λ), we obtain the ratio of k_{ext} at the two wavelengths and square it, obtaining

$$\left[\frac{k_{\text{ext}}(\lambda_1)}{k_{\text{ext}}(\lambda_0)}\right]^2 \approx \frac{(1-\bar{\omega})_1}{(1-\bar{\omega})_0}. \quad (12)$$

We next argue that the single-scattering coalbedo $(1 - \bar{\omega})$ of a snow grain is proportional to the absorption coefficient of pure ice, k_{ice}, for the visible and near UV. From Eq. (6), the single-scattering coalbedo is $Q_{\text{abs}}/Q_{\text{ext}}$, the probability that a photon will be absorbed rather than scattered when it interacts with a

particle. For $r \gg \lambda$, ray-tracing arguments are appropriate, so radiation is attenuated exponentially as it passes through the particle:

$$Q_{\text{abs}} \propto 1 - \exp(-r_i k_{\text{ice}}) \approx r_i k_{\text{ice}} \tag{13}$$

for $r_i k_{\text{ice}} \ll 1$, which is valid for our situation. For example, for $r = 50\ \mu\text{m}$ and $\lambda = 600\ \text{nm}$, $r_i k_{\text{ice}} \approx 5 \times 10^{-7}$. A rigorous derivation by Bohren and Huffman[49] (their Eq. 7.2) shows that $Q_{\text{abs}} \sim r_i k_{\text{ice}}$ for weakly absorbing spheres that are large compared to the wavelength. We therefore expect $Q_{\text{abs}} \sim r_i k_{\text{ice}}$ and, because Q_{ext} is independent of wavelength,

$$(1 - \bar{\omega}) \sim r_i k_{\text{ice}}. \tag{14}$$

We tested this hypothesis by carrying out Mie calculations for the snow grain radii characteristic of Antarctic surface snow, 40–200 μm, and found that the ratio $(1 - \bar{\omega})/(r_i k_{\text{ice}})$ was nearly constant, varying from 0.88 for $r_i = 40\ \mu\text{m}$ to 0.85 for $r_i = 200\ \mu\text{m}$. The ratio is independent of wavelength to within 1% for all values of k_{ice} up to $2\ \text{m}^{-1}$. [This covers all wavelengths we consider; our maximum value is $k_{\text{ice}} = 0.12\ \text{m}^{-1}$ at $\lambda_0 = 600\ \text{nm}$, so approximation (14) is verified.] The average grain size in a layer is independent of wavelength, so $(1 - \bar{\omega}) \sim k_{\text{ice}}$. We therefore conclude from approximation (12) that

$$\left[\frac{k_{\text{ext}}(\lambda)}{k_{\text{ext}}(\lambda_0)}\right]^2 \approx \frac{k_{\text{ice}}(\lambda)}{k_{\text{ice}}(\lambda_0)}, \tag{15}$$

where k_{ext} is the measured flux extinction coefficient in snow, from the slopes in Fig. 3, and $k_{\text{ice}}(\lambda_0)$ is the known absorption coefficient of pure ice at $\lambda_0 = 600\ \text{nm}$. We use approximation (15) to infer $k_{\text{ice}}(\lambda)$ for wavelengths $\lambda < 600\ \text{nm}$.

B. Results

The results are shown in Fig. 5 and are compared with the AMANDA and laboratory results that were shown in Fig. 1. For layer C we have only one usable hole, but for layer B there are three. The average of the three holes is shown, along with maximum and minimum values at each wavelength. The wavelength of minimum absorption is 390 nm. Our results for layer B agree with AMANDA at 1755 m, whereas our results for layer C are lower than the lowest AMANDA values. As shown by the AMANDA workers,[9,17] the absorption coefficient of pure ice is probably lower than all these curves, and their spread is due to different amounts of absorptive impurities, which have little effect on the inferred absorption coefficient at $\lambda = 600\ \text{nm}$ but cause significant discrepancies at shorter wavelengths. However, for the wavelength of minimum absorption, our finding that $\lambda_{\text{min}} = 390\ \text{nm}$ agrees with the judgment of the AMANDA workers, based on their extrapolation of the data for their cleanest ice at 830 m depth (Fig. 19 of Ref. 11).

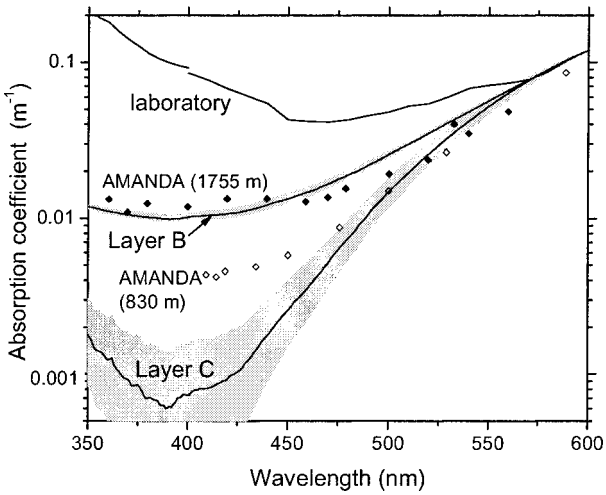

Fig. 5. Spectral absorption coefficient of ice, inferred from the snow transmission measurements for layers B and C, before removing the absorption by impurities. The values for layer C are lower because layer C consists of snow that fell before establishment of the station in 1997, so it contains less soot than layer B. Accurate measurements for layer B were obtained in three holes on three different days. The average of the three holes is shown, along with maximum and minimum values at each wavelength. (This spread is similar to the uncertainty in the slopes in Fig. 3 for individual holes.) Values from the laboratory measurements and from two depths of the AMANDA experiment (filled and open symbols) are shown for comparison. The shaded region surrounding the curve for layer C is propagated from the shaded region of Fig. 4(b), representing the uncertainty in the slopes of the transmission plots of Fig. 3.

The conclusion that our derived absorption coefficients are affected by impurities in the snow could already be inferred from Fig. 4(b) as follows. Taking the ratio of k_{ext} from Eq. (7) in two layers (rather than two wavelengths), where k_B and k_C are values of k_{ext} in layers B and C, with grain radii r_B and r_C,

$$\left(\frac{k_B}{k_C}\right)^2 = \frac{\sigma_B{}^2(1 - \bar{\omega})_B}{\sigma_C{}^2(1 - \bar{\omega})_C}. \tag{16}$$

Using the grain-size dependences of σ_{ext} and $(1 - \bar{\omega})$ from Eqs. (11) and (14),

$$\left(\frac{k_B}{k_C}\right)^2 = \left(\frac{r_C}{r_B}\right)^2 \frac{r_B}{r_C} = \frac{r_C}{r_B}. \tag{17}$$

Since r_C and r_B are independent of λ, $(\log k_B - \log k_C)$ should be a constant, and the two curves in Fig. 4(b) should have a constant offset. The fact that they do not is an indication that $(1 - \bar{\omega})$ is not just proportional to r_i, and that there is another absorber in the snow in addition to ice. The curves do have a nearly constant offset for 550–600 nm, where absorption is dominated by ice rather than impurities.

We offer the lowest curve in Fig. 5 (layer C) as an upper limit to the absorption coefficient of pure ice because it attributes all of the snow's absorption to ice at all wavelengths. In Appendix A we attempt to find

a lower limit to k_{ice} by assigning all the absorption at λ_{min} to impurities.

We note that our inferred absorption coefficient agrees with AMANDA's at $\lambda = 550$ nm, so an alternative to using $\lambda_0 = 600$ nm would be to use $\lambda_0 = 550$ nm with AMANDA's k_{ice}; this would avoid dependence on the extrapolation to 600 nm shown in Fig. 4 and would give the same results for $k_{ice}(\lambda)$ as those shown in Fig. 5.

The disturbance to the radiation field caused by the hole was calculated by Light[50] using the method of Ref. 51; the effect on our inferred k_{ice} at 390 nm, due to possible leakage of light along the walls of the hole, was very small. Any leakage of light would cause the measured k_{ext} to be smaller than that in undisturbed snow by a larger factor at the more absorptive reference wavelength than at 390 nm. Then from approximation (15), k_{ice} at 390 nm would be overestimated. The consideration of leakage is therefore another reason for considering our inferred k_{ice} to be an upper limit.

5. Accounting for Absorptive Impurities

A. Measurement of Soot in Snow

Antarctic snow is very clean, but ice is so weakly absorptive in the visible and near UV that impurities can dominate the absorption. The AMANDA measurements at 1755 m were made in ice that fell as snow during the last ice age, when the rate of dust deposition was considerably greater than at present.[52] The ice at 830 m was deposited at the beginning of the Holocene (10,000 years ago), when the dust deposition rate was approximately the same as at present. The dust content in modern snow at Dome C is ~26 ng/g of snow (26 ppb)[52] and at the South Pole it is 15 ppb.[53] In addition to soil dust, there is soot, which consists of carbon and hydrogen in submicrometer particles resulting from incomplete combustion. Soot is present in a lower concentration than dust, but it can dominate the absorption because, for the sizes of soot and dust particles found in snow, soot is ~50 times as absorptive as the same mass of dust.[32,54] Surveys of the soot content of snow around South Pole Station[27] and Vostok Station[2] found peak values downwind of the station. Background levels 10–13 km upwind of these stations were 0.1–0.3 ppb at the South Pole and 0.6 ppb at Vostok; the difference is consistent with the factor of 3 difference in snow accumulation rates (7 g cm^{-2} yr^{-1} at the South Pole; 2.5 at Vostok) assuming the same fallout rate of soot.

We measured absorptive impurities in snow at our transmission sites at Dome C, using the method of Warren and Clarke.[27] Snow was collected in glass jars and kept frozen until it was melted rapidly in a microwave oven (to reduce the probability of soot sticking to the glass); the meltwater was then filtered. The filters were compared visually with standard filters with known soot amounts, and later measured in the laboratory with an integrating plate photometer at four visible wavelengths. Absorption by the filters was nearly independent of wavelength, indicating that the dominant absorber was soot (which is gray) rather than dust (red).

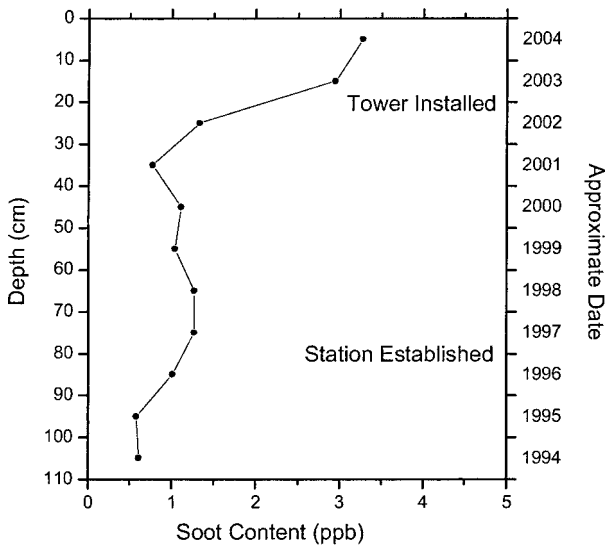

Fig. 6. Soot content of snow at Dome C, as a function of depth, from the surface down to 105 cm. The corresponding approximate ages of snow are given on the right-hand scale. Snow was sampled on 18 January 2005, at the location where the measurements of transmission (Fig. 3) were made on 5 January.

There is ongoing research to determine the optical properties of soot.[55,56] To convert our filter absorption measurement to effective soot concentration C (which accounts for the absorption of light by all impurities, not just soot), we assumed a mass absorption cross section $\beta_{abs} = 6$ m^2/g at $\lambda = 550$ nm, which was the value for the soot on the calibration-standard filters. However, since the filter measurement is a light absorption measurement and our application is to compute light absorption in snow, the actual value of specific absorption assumed is not important, as long as the same value is used in the radiative transfer model of soot in snow (below). The results are shown in Fig. 6 for snow at the 5 January site, where the transmission measurements for Fig. 3 were made, 200 m north of the tower. The soot content in layer C was constant at $C_C \approx 0.6$ ppb, in agreement with the background concentration 10 km upwind of Vostok. However, this value is close to the detection limit for the quantity of meltwater filtered, so it is highly uncertain. Between 30 and 90 cm (layer B), the average (C_B) was ~1.2 ppb, indicating some contamination from station activities. The topmost snow, 0–30 cm, shows higher values because of activities at the tower in 2003–2004, but it does not affect our estimates of k_{ext}, which used $z_0 \geq 30$ cm.

There is some uncertainty in relating the radiative effects of soot in snow to the radiative effects of soot on a filter. The absorptive properties of soot particles depend on the refractive index of the surrounding medium. A soot particle on the surface of the nuclepore filter material may not have the same mass absorption cross section as a soot particle on the sur-

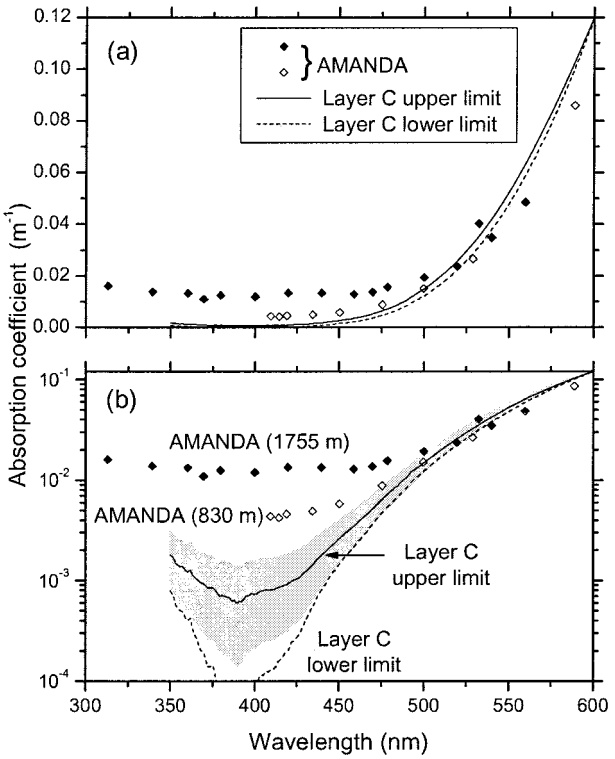

Fig. 7. Spectral absorption coefficient of ice on both (a) linear and (b) logarithmic scales, inferred from the snow transmission measurements after subtraction of the absorption by impurities (assumed to be soot). The upper (solid) curve in each frame results from attributing all the absorption to ice, and is identical to the lowest curve in Fig. 5. We propose this curve (with its uncertainties) as an upper bound to the true spectral absorption coefficient of pure ice. The lower (dashed) curve results from the analysis in Appendix A, assuming that ice is nonabsorptive at $\lambda = 390$ nm, so that all the absorption at that wavelength is caused by impurities. It is a suggested lower bound to the spectral absorption coefficient of ice. The AMANDA results from the two depths shown here are the same as those in Fig. 5. The shaded region surrounding the upper-limit curve is propagated from the shaded region of Fig. 4(b), representing the uncertainty in the slopes of the transmission plots of Fig. 3.

face of a snow grain. Another potentially significant difference is that the soot particles are on the surface of the filter but may be embedded within the snow particles. The resulting difference between β_{abs}(filter) and β_{abs}(snow) is at most a factor of 2.[57,58]

B. Effect of Soot on Inferred Absorption by Ice

The spectral absorption coefficient of pure ice is probably lower than the values shown in Fig. 5 for layer C, because impurities were responsible for some of the measured absorption. In Appendix A we develop a method to account for absorption by impurities by comparing the values of k_{ext} in layer B with those in layer C, and derive both upper and lower limits to $k_{ice}(\lambda)$. The upper limit is that shown in Fig. 5 for layer C. The lower limit results from attributing all the absorption to impurities at the wavelength of minimum absorption (390 nm). The results are shown in Fig. 7. The upper-limit values, after 10-point smoothing, are listed in Table 2, together with their uncertainties.

Table 2. Upper Limit for Absorption Coefficient of Pure Ice, Obtained from Snow Transmission Measurements in Layer C[a]

λ (nm)	k_{ice} (m^{-1})	k_{ice}^{-} (m^{-1})	k_{ice}^{+} (m^{-1})
350	1.78×10^{-3}	8.38×10^{-4}	3.08×10^{-3}
355	1.45×10^{-3}	6.48×10^{-4}	2.60×10^{-3}
360	1.25×10^{-3}	5.12×10^{-4}	2.33×10^{-3}
365	1.08×10^{-3}	4.02×10^{-4}	2.08×10^{-3}
370	9.21×10^{-4}	3.11×10^{-4}	1.86×10^{-3}
375	8.11×10^{-4}	2.49×10^{-4}	1.70×10^{-3}
380	7.31×10^{-4}	2.06×10^{-4}	1.59×10^{-3}
385	6.60×10^{-4}	1.71×10^{-4}	1.47×10^{-3}
390	6.38×10^{-4}	1.63×10^{-4}	1.43×10^{-3}
395	6.79×10^{-4}	1.83×10^{-4}	1.50×10^{-3}
400	7.43×10^{-4}	2.17×10^{-4}	1.59×10^{-3}
405	7.82×10^{-4}	2.40×10^{-4}	1.64×10^{-3}
410	8.18×10^{-4}	2.61×10^{-4}	1.69×10^{-3}
415	8.62×10^{-4}	2.86×10^{-4}	1.75×10^{-3}
420	9.38×10^{-4}	3.31×10^{-4}	1.86×10^{-3}
425	1.04×10^{-3}	3.96×10^{-4}	2.01×10^{-3}
430	1.21×10^{-3}	5.04×10^{-4}	2.24×10^{-3}
435	1.47×10^{-3}	6.76×10^{-4}	2.59×10^{-3}
440	1.79×10^{-3}	8.95×10^{-4}	3.00×10^{-3}
445	2.15×10^{-3}	1.16×10^{-3}	3.47×10^{-3}
450	2.58×10^{-3}	1.48×10^{-3}	4.01×10^{-3}
455	3.05×10^{-3}	1.84×10^{-3}	4.59×10^{-3}
460	3.62×10^{-3}	2.28×10^{-3}	5.28×10^{-3}
465	4.33×10^{-3}	2.85×10^{-3}	6.13×10^{-3}
470	5.23×10^{-3}	3.59×10^{-3}	7.21×10^{-3}
475	6.29×10^{-3}	4.47×10^{-3}	8.46×10^{-3}
480	7.49×10^{-3}	5.48×10^{-3}	9.84×10^{-3}
485	8.91×10^{-3}	6.71×10^{-3}	1.15×10^{-2}
490	1.07×10^{-2}	8.25×10^{-3}	1.35×10^{-2}
495	1.27×10^{-2}	9.99×10^{-3}	1.57×10^{-2}
500	1.48×10^{-2}	1.18×10^{-2}	1.82×10^{-2}
505	1.72×10^{-2}	1.39×10^{-2}	2.09×10^{-2}
510	1.98×10^{-2}	1.62×10^{-2}	2.39×10^{-2}
515	2.28×10^{-2}	1.89×10^{-2}	2.71×10^{-2}
520	2.60×10^{-2}	2.18×10^{-2}	3.07×10^{-2}
525	2.96×10^{-2}	2.51×10^{-2}	3.45×10^{-2}
530	3.34×10^{-2}	2.87×10^{-2}	3.87×10^{-2}
535	3.76×10^{-2}	3.26×10^{-2}	4.32×10^{-2}
540	4.22×10^{-2}	3.69×10^{-2}	4.80×10^{-2}
545	4.71×10^{-2}	4.16×10^{-2}	5.31×10^{-2}
550	5.23×10^{-2}	4.67×10^{-2}	5.84×10^{-2}
555	5.78×10^{-2}	5.21×10^{-2}	6.40×10^{-2}
560	6.37×10^{-2}	5.80×10^{-2}	6.99×10^{-2}
565	6.99×10^{-2}	6.43×10^{-2}	7.59×10^{-2}
570	7.63×10^{-2}	7.10×10^{-2}	8.21×10^{-2}
575	8.31×10^{-2}	7.81×10^{-2}	8.84×10^{-2}
580	9.01×10^{-2}	8.56×10^{-2}	9.48×10^{-2}
585	9.73×10^{-2}	9.36×10^{-2}	1.01×10^{-1}
590	1.05×10^{-1}	1.02×10^{-1}	1.08×10^{-1}
595	1.12×10^{-1}	1.11×10^{-1}	1.14×10^{-1}
600	1.20×10^{-1}	1.20×10^{-1}	1.20×10^{-1}

[a]The values are a smoothed version of the plot in Fig. 7(b) (also shown in Fig. 5). This upper limit is obtained by assuming that all the absorption at all wavelengths is due to ice. The central estimate of this upper limit is k_{ice}, a smoothed version of the upper-limit line in Fig. 7(b). Uncertainty in the linear slopes in Fig. 3 propagates to a range of values from k_{ice}^{-} to k_{ice}^{+}, corresponding to 1 standard deviation of the slope estimate. The values of k_{ice}^{-} and k_{ice}^{+} listed here are smoothed boundaries of the shaded region in Fig. 7(b).

It is puzzling that AMANDA's ice at 830 m appears to contain more absorptive impurities than the surface snow at Dome C because the dust content of surface snow at the South Pole (15 ppb, Ref. 53) is lower than that at Dome C (26 ppb, Ref. 52), and the concentration of dust in a Dome C ice core is rather constant through the Holocene,[52] which should include the 830 m ice at the South Pole. The 830 m ice at the South Pole is dated at approximately 10,000 years ago,[59] and the dust content at Dome C dropped to its Holocene values at ~13,000 years ago. However, we cannot rule out the possibility that the dust content at 830 m exceeds that in surface snow. Alternatively, it may be that our low values of inferred k_{ice} are the result of experimental error, and that our error bars (the shaded region of Fig. 7) are too small. It will therefore be important to repeat the snow transmission experiment at other locations. If our low value of k_{ice} is correct, it would not require radically different conclusions about the dust content in the South Pole ice; for example, the inferred dust content at 1755 m would have to be increased by just one third (assuming that the dust at 1755 m has the same composition as the dust at 830 m).

6. Comparison of Ice with Liquid Water

Like ice, liquid water also has its absorption minimum near the UV–visible boundary. The most accurate measurements of the absorption coefficient of liquid water in this spectral region are those of Pope and Fry,[60] who used two methods that infer absorption using measurements that are unaffected by scattering. Their minimum absorption was 0.0044 m^{-1} at $\lambda_{\mathrm{min}} = 418$ nm. Our inferred k_{ice} is lower and shifted to a shorter wavelength by 30 nm, to 390 nm. [The AMANDA workers also estimate $\lambda_{\mathrm{min}} \approx 390$ nm for their cleanest ice (Fig. 19 of Ref. 11).] This shift may indicate that the Urbach tail (the steep decline of absorption from the UV toward the visible, seen in Minton's measurements in Fig. 1, discussed in Subsection 4.A of Ref. 9) is steeper for the crystalline material (ice) than for the amorphous material (liquid water).

7. Conclusion

Our measurements of spectral transmission in snow find the wavelength of minimum absorption at 390 nm, consistent with the AMANDA results. We find an upper bound to the spectral absorption coefficient of pure ice (k_{ice}) for the wavelength region 350–600 nm, which is lower than the lowest AMANDA values for 350–500 nm, and much lower than the laboratory measurements. We therefore agree with the conclusions of the AMANDA group: (a) The laboratory measurements of attenuation for $\lambda < 600$ nm were significantly affected by scattering, and at shorter wavelengths the measured attenuation was almost entirely due to scattering. (b) In the clear ice measured by AMANDA deep within the ice sheet at the South Pole, the absorption at $\lambda < 500$ nm was dominated by impurities.

At 390 nm we find an upper limit to k_{ice} in the range of 2–14 $\times$ 10^{-4} m^{-1} (Table 2), corresponding to an absorption length of 700–6000 m. By comparison, the absorption length for ice at 390 nm reported from the laboratory measurements was 10 m, and for AMANDA's cleanest ice it was 240 m. This result is tentative; we are skeptical of our low k_{ice} because there is reason to think that the ice at 830 m depth at the South Pole probably does not contain more dust than the surface snow at Dome C.

Our analysis required an evaluation of the effect of impurities (soot) on our measured spectral transmission. This complication was not anticipated. We had measured the soot content and knew that it was too small to affect the albedo measurably; it was not until after completion of the field experiment that its significant effect on transmission became apparent. We did reach background concentrations of soot in layer C, below the 1997 level (when the station was established), so we used this layer for our analyses. Wavelengths longer than 550 nm did not penetrate far enough into this layer to be analyzed, requiring us either to use a complex procedure to derive the required extinction coefficient at the reference wavelength of 600 nm, or to assume that the AMANDA result at 550 nm was accurate for pure ice. Both approaches gave the same result. It would be good to repeat this experiment at a site much farther from the station than our 2 km site, where even the surface snow would be as clean as layer C. Snow even cleaner than layer C could be sampled in regions of Antarctica that have greater snow accumulation rates.

Because our analysis was limited to one experiment, our quantitative results are tentative. However, the method appears to be capable of obtaining accurate absorption coefficients for ice in the visible and near UV, particularly if impurities can be kept to low levels.

Appendix A: Accounting for Absorption by Soot in Analysis of Extinction Coefficients

The differences in k_{ext} between layers B and C in Fig. 4 are due to their different soot contents C and to their different average grain radii r_i. However, the relative effects of r_i and C on k_{ext} vary with wavelength. We will exploit this variation, together with the constraints that r_B, r_C, and $(C_B - C_C)$ are independent of wavelength, to obtain all three quantities from the radiation measurements.

In this analysis we assume that both r_i and C are different in the two layers, but that they are constant within each layer. The justification for this assumption is that the transmission data in Fig. 3 can be fitted with two straight lines. The visual estimates of grain size are highly uncertain, and the radiative effect of soot is also uncertain, and there are only two data points for C_C below 90 cm in Fig. 6. Our strategy therefore is to estimate values for r_i and C from the snow transmission measurements alone. We will con-

clude that $r_B \approx 43$ μm, $r_C \approx 135$ μm, $C_B \approx 3$ ppb, and $C_C \approx 0.3$ ppb.

If ice were sufficiently absorptive at $\lambda_0 = 600$ nm to dominate the absorption at that wavelength, we could assume that $k_{\text{ext}}(\lambda_0)$ is unaffected by soot. However, our analysis below (after iteration) converges on the conclusion that soot is responsible for 9% of the 600 nm absorption in layer B and 0% in layer C, so we will include those values in the derivation that commences here.

Mie calculations were performed for ice spheres of various radii to obtain Q_{ext}, $\bar{\omega}$, and g; those values were put into Eqs. (11) and (7) to compute k_{ext}. The measured values of k_{ext} for 600–608 nm correspond to a grain size $r_B = 43 \pm 2$ μm (after adjusting by 9% for the soot contribution; it would be 47 μm if soot were ignored). (This result is consistent with our measurement of snow grain sizes on photographs. It is also consistent with the spectral albedo we measured at Dome C: In the near IR, where the albedo is sensitive to grain size, the measured albedo implies a surface grain radius of ~50 μm.)

We define ρ_s = density of soot; ρ_i = density of ice; r_i, r_s = effective radii of ice particles, soot particles; n_i, n_s = number density of ice particles, soot particles; X_m = geometric cross-sectional area per unit mass for a soot particle.

The mass concentration C of soot in snow (grams of soot per gram of snow) is related to the above quantities by

$$C = \frac{\frac{4}{3}\pi {r_s}^3 \rho_s n_s}{\frac{4}{3}\pi {r_i}^3 \rho_i n_i} = \frac{3 n_s {r_s}^2}{4 n_i {r_i}^3 \rho_i X_m}. \quad \text{(A1)}$$

For a snowpack that contains both ice particles and soot particles, the single-scattering coalbedo is

$$(1 - \bar{\omega}) = \frac{{\sigma_{\text{abs}}}^{\text{soot}} + {\sigma_{\text{abs}}}^{\text{ice}}}{{\sigma_{\text{ext}}}^{\text{soot}} + {\sigma_{\text{ext}}}^{\text{ice}}}. \quad \text{(A2)}$$

The extinction coefficient σ_{ext} (units of m^{-1}) is the product of the unitless extinction efficiency, the cross-sectional area of a particle, and the number density of particles, as in Eq. (8) and similarly for the absorption coefficient σ_{abs}. For soot concentrations of the order of parts per billion, ${\sigma_{\text{ext}}}^{\text{soot}} \ll {\sigma_{\text{ext}}}^{\text{ice}}$. Equation (A2) then becomes

$$(1 - \bar{\omega}) = \frac{n_s \pi {r_s}^2 {Q_{\text{abs}}}^{\text{soot}} + n_i \pi {r_i}^2 {Q_{\text{abs}}}^{\text{ice}}}{n_i \pi {r_i}^2 {Q_{\text{ext}}}^{\text{ice}}}. \quad \text{(A3)}$$

As noted just below Eq. (11), ${Q_{\text{ext}}}^{\text{ice}}$ is independent of wavelength for our domain of interest. Now we use Eq. (A3) at two wavelengths λ_0 and λ_1 (where $\lambda_0 = 600$ nm) and take the ratio,

$$\frac{(1 - \bar{\omega})_1}{(1 - \bar{\omega})_0} = \frac{\frac{n_s {r_s}^2}{n_i {r_i}^2} {Q_{\text{abs}}}^{\text{soot}}(\lambda_1) + {Q_{\text{abs}}}^{\text{ice}}(\lambda_1)}{\frac{n_s {r_s}^2}{n_i {r_i}^2} {Q_{\text{abs}}}^{\text{soot}}(\lambda_0) + {Q_{\text{abs}}}^{\text{ice}}(\lambda_0)}. \quad \text{(A4)}$$

At 600 nm, where ice is relatively absorptive, absorption by the small amount of soot in the snow is much less than the absorption by ice. Therefore, in the denominator of Eq. (A4), the first term is small compared with the second term. We assume it is 9% of the second term in layer B and 0% in layer C; this assumption is confirmed below. With these assumptions, and substituting for $n_s {r_s}^2 / n_i {r_i}^2$ from Eq. (A1) and using approximation (12), we obtain

$$\left(\frac{k_1}{k_0}\right)^2 = \frac{\frac{4}{3} r_i \rho_i X_m C {Q_{\text{abs}}}^{\text{soot}}(\lambda_1) + {Q_{\text{abs}}}^{\text{ice}}(\lambda_1)}{f {Q_{\text{abs}}}^{\text{ice}}(\lambda_0)}, \quad \text{(A5)}$$

where $f = 1.09$ for layer B and 1.00 for layer C, and the left-hand side is the ratio of flux extinction coefficients, obtained from the snow transmission measurements by Eq. (3).

From the discussion of approximation (14), $(1 - \bar{\omega})_{\text{ice}} = 0.88 k_{\text{ice}} r_i$. We also have ${Q_{\text{ext}}}^{\text{ice}} = 2.03$, so

$${Q_{\text{abs}}}^{\text{ice}} = (2.03)(0.88) k_{\text{ice}} r_i = 1.79 k_{\text{ice}} r_i. \quad \text{(A6)}$$

Putting Eq. (A6) into Eq. (A5) and canceling r_i,

$$1.79 f k_{\text{ice}}(\lambda_0)\left(\frac{k_1}{k_0}\right)^2 = \frac{4}{3} \rho_i X_m C {Q_{\text{abs}}}^{\text{soot}}(\lambda_1) + 1.79 k_{\text{ice}}(\lambda_1). \quad \text{(A7)}$$

At $\lambda_0 = 600$ nm, $k_{\text{ice}} = 0.12\ \text{m}^{-1}$.[5] The assumption in the filter analysis of soot is $\beta_{\text{abs}} = {Q_{\text{abs}}}^{\text{soot}} X_m = 6\ \text{m}^2\text{g}^{-1}$. We assume that β_{abs} is independent of wavelength. This is not true for fresh soot,[55] but it does appear to be approximately true for soot in snow.[61] The reason for the lack of wavelength dependence for absorption by aged soot in snow may be its clumping into larger particles.[62]

With these values, Eq. (A7) simplifies to

$$a f \left(\frac{k_1}{k_0}\right)^2 = C + b k_{\text{ice}}(\lambda_1), \quad \text{(A8)}$$

where $a = 2.93 \times 10^{-8}$ and $b = 2.44 \times 10^{-7}$ m.

We next relate $k_{\text{ext}}(\lambda_0)$ for layer B to that of layer C. We will use Eqs. (A5) and (A8) for both upper and lower layers; both C and r_i will differ for the two layers. For example, for layer B we would replace the quantities (k_1, r_i, C, f) in Eq. (A5) by (k_B, r_B, C_B, f_B). At λ_0 we can use Eqs. (16) and (17), modified by including f: From Eqs. (16) and (17), with $(1 - \bar{\omega})_0 = 0.88 k_{\text{ice}} r_i f$, we obtain

$$\frac{{k_{0B}}^2}{{k_{0C}}^2} = \frac{r_C f_B}{r_B f_C}. \tag{A9}$$

Writing Eq. (A8) for the upper and lower layers, then subtracting the two equations and substituting $f_C/{k_{0C}}^2$ from Eq. (A9), we obtain

$$\frac{a f_B}{{k_{0B}}^2}\left[{k_{1B}}^2 - {k_{1C}}^2 \frac{r_C}{r_B}\right] = C_B - C_C. \tag{A10}$$

But $(C_B - C_C)$ must be independent of wavelength, so the quantity in brackets must also be independent of wavelength. This quantity was computed at all wavelengths for various choices of r_C/r_B; an excellent fit was found for $r_C/r_B = 3.14$. Since $r_B = 43$ μm, we obtain $r_C = 135$ μm.

Putting these values into Eq. (A9), with $f_B = 1.09$, $f_C = 1.00$, and the measured value of $k_{0B} = 0.262$ m^{-1} (Fig. 4), we obtain $k_{0C} = 0.141$ m^{-1}. This is the value plotted in Fig. 4 for layer C at $\lambda = 600$ nm. It does appear to be consistent with the extrapolated trend of experimental values for 500–550 nm.

Putting the value of r_C/r_B into Eq. (A10), we obtain $(C_B - C_C) = 2.5$ ppb. This value is inconsistent with the measurements in Fig. 6. We attribute this inconsistency to a possible factor of 2 enhancement of β_{abs} on the filter, as mentioned above, together with a possible overestimate of C_C, which was just at the detection limit of measurement.

This analysis gives only the difference between C_B and C_C, not their individual values. Bounds to C_C can be set by assuming that $C_C = 0$ or alternatively that soot is responsible for all the absorption at λ_{min}. When we assume $C_C = 0$, Eq. (A5) gives $k_{\mathrm{ice}}(\lambda)$ identical to the values obtained above using approximation (15) for layer C, plotted in Fig. 5, because Eq. (A5) reduces to approximation (15) for this case. This gives an upper limit for $k_{\mathrm{ice}}(\lambda)$.

The lower limit on $k_{\mathrm{ice}}(\lambda)$ is obtained by setting $k_{\mathrm{ice}} = 0$ at $\lambda_{\mathrm{min}} = 390$ nm. Then Eq. (A8) reduces to

$$a f_C \left[\frac{k_{1C}(390\ \mathrm{nm})}{k_{0C}(390\ \mathrm{nm})}\right]^2 = C_C. \tag{A11}$$

Using the values of $k_{\mathrm{ext}}(\lambda)$ for layer C from Fig. 4, we obtain $C_C = 0.3$ ppb. This is not an unreasonable value; it is similar to the values found in remote snow 13 km upwind of the South Pole (0.1–0.3 ppb).[27]

Putting this value of C_C into Eq. (A8) we obtain a lower limit for $k_{\mathrm{ice}}(\lambda)$. Both upper and lower limits are plotted in Fig. 7. Because of the uncertainties in the wavelength dependence of soot absorption, the lower limit is rather uncertain. The upper-limit values from Fig. 7, after 10-point smoothing, are listed in Table 2.

Finally, with C_B in the range of 2.5–2.8 ppb, together with $r_B = 43$ μm, which has ${Q_{\mathrm{abs}}}^{\mathrm{ice}} = 9.4 \times 10^{-6}$ at 600 nm, we evaluate the denominators of Eqs. (A4) and (A5) and verify that $f_B = 1.09$ and $f_C = 1.00$ as anticipated.

We thank Matthew Sturm and William Simpson for the idea of measuring transmission using a vertical probe instead of a snow-pit wall, and Delphine Six for persuading us to measure soot at Dome C. We thank Stephen Hudson for his assistance with the preliminary measurements in December 2003 and Tami Bond for discussions about soot. Bonnie Light computed the disturbance of the radiation field caused by the hole. We thank Michel Fily (Laboratoire de Glaciologie et Géophysique de l'Environnement, Grenoble, France) for sponsoring our project, and the Dome C crew for support. Logistics at Dome C were provided by the French and Italian Antarctic Programs: Institut Polaire Français Paul Emile Victor (IPEV) and Programma Nazionale di Ricerche in Antartide (PNRA). Helpful comments were obtained from Stephen Hudson on the first draft and from an anonymous reviewer on the submitted draft. The research was supported by National Science Foundation grant OPP-00-03826.

References

1. S. G. Warren, "Optical constants of ice from the ultraviolet to the microwave," Appl. Opt. **23,** 1206–1225 (1984).
2. T. C. Grenfell, S. G. Warren, and P. C. Mullen, "Reflection of solar radiation by the Antarctic snow surface at ultraviolet, visible, and near-infrared wavelengths," J. Geophys. Res. **99,** 18669–18684 (1994).
3. S. G. Warren, R. E. Brandt, T. C. Grenfell, and C. P. McKay, "Snowball Earth: ice thickness on the tropical ocean," J. Geophys. Res. (Oceans) **107C,** 3167, doi:10.1029/2001JC001123 (2002).
4. F. Sauberer, "Die spektrale Strahlungsdurchlässigkeit des Eises" [The spectral transmissivity of ice] Wetter Leben **2,** 193–197 (1950).
5. T. C. Grenfell and D. K. Perovich, "Radiation absorption coefficients of polycrystalline ice from 400 to 1400 nm," J. Geophys. Res. **86,** 7447–7450 (1981).
6. D. K. Perovich and J. W. Govoni, "Absorption coefficients of ice from 250 to 400 nm," Geophys. Res. Lett. **18,** 1233–1235 (1991).
7. P. B. Price and L. Bergström, "Optical properties of deep ice at the South Pole: scattering," Appl. Opt. **36,** 4181–4194 (1997).
8. P. Askebjer, S. W. Barwick, L. Bergström, A. Bouchta, S. Carius, E. Dalberg, B. Erlandsson, A. Goobar, L. Gray, A. Hallgren, F. Halzen, H. Heukenkamp, P. O. Hulth, S. Hundertmark, J. Jacobsen, V. Kandhadai, A. Karle, I. Liubarsky, D. Lowder, T. Miller, P. Mock, R. Morse, R. Porrata, P. B. Price, A. Richards, H. Rubinstein, E. Schneider, Ch. Spiering, O. Streicher, Q. Sun, Th. Thon, S. Tilav, R. Wischnewski, C. Walck, and G. Yodh, "UV and optical light transmission properties in deep ice at the South Pole," Geophys. Res. Lett. **24,** 1355–1358 (1997).
9. P. Askebjer, S. W. Barwick, L. Bergström, A. Bouchta, S. Carius, E. Dalberg, K. Engel, B. Erlandsson, A. Goobar, L. Gray, A. Hallgren, F. Halzen, H. Heukenkamp, P. O. Hulth, S. Hundertmark, J. Jacobsen, A. Karle, V. Kandhadai, I. Liubarsky, D. Lowder, T. Miller, P. Mock, R. M. Morse, R. Porrata, P. B. Price, A. Richards, H. Rubinstein, E. Schneider, Ch. Spiering, O. Streicher, Q. Sun, Th. Thon, S. Tilav, R. Wischnewski, C. Walck, and G. B. Yodh, "Optical properties of deep ice at the South Pole: absorption," Appl. Opt. **36,** 4168–4180 (1997).
10. K. Woschnagg, "Optical properties of South Pole ice at depths from 140 to 2300 meters," in *Proceedings of the 26th International Cosmic Ray Conference,* B. L. Dingus, D. B. Kieda, and M. H. Salamon, eds. (American Institute of Physics, 2000), Vol. 2, pp. 200–203.
11. K. Woschnagg, Department of Physics, 366 LeConte Hall, Uni-

versity of California, Berkeley, Calif. 94720, and the AMANDA collaboration have submitted a manuscript called "Optical properties of deep glacial ice at the South Pole" to the Journal of Geophysical Research.
12. A. Minton, "The far-ultraviolet spectrum of ice," J. Phys. Chem. **75,** 1162–1164 (1971).
13. H. K. Hughes, "Suggested nomenclature in applied spectroscopy," Anal. Chem. **24,** 1349–1354 (1952).
14. A. Minton, National Institutes of Health, Bethesda, Maryland (personal communication, 1985).
15. S. G. Warren and E. P. Shettle, "Optical constants of ice in the infrared atmospheric windows," in *Sixth Conference on Atmospheric Radiation* (American Meteorological Society, 1986), pp. 103–106.
16. K. Woschnagg and P. B. Price, "Temperature dependence of absorption in ice at 532 nm," Appl. Opt. **40,** 2496–2500 (2001).
17. Y. D. He and P. B. Price, "Remote sensing of dust in deep ice at the South Pole," J. Geophys. Res. **103,** 17041–17056 (1998).
18. I. Allison, R. E. Brandt, and S. G. Warren, "East Antarctic sea ice: albedo, thickness distribution and snow cover," J. Geophys. Res. (Oceans) **98,** 12417–12429 (1993).
19. T. Aoki, T. Aoki, M. Fukabori, A. Hachikubo, Y. Tachibana, and F. Nishio, "Effects of snow physical parameters on spectral albedo and bidirectional reflectance of snow surface," J. Geophys. Res. **105,** 10219–10236 (2000).
20. S. G. Warren, R. E. Brandt, and R. D. Boime, "Blue ice and green ice," Antarct. J. U.S. **28,** 255–256 (1993).
21. R. E. Brandt, S. G. Warren, A. P. Worby, and T. C. Grenfell, "Surface albedo of the Antarctic sea-ice zone," J. Clim. **18,** 3606–3622 (2005).
22. S. G. Warren, C. S. Roesler, and R. E. Brandt, "Solar radiation processes in the East Antarctic sea ice zone," Antarct. J. U.S. **32,** 185–187 (1997).
23. S. G. Warren, C. S. Roesler, V. I. Morgan, R. E. Brandt, I. D. Goodwin, and I. Allison, "Green icebergs formed by freezing of organic-rich seawater to the base of Antarctic ice shelves," J. Geophys. Res. **98,** 6921–6928 and 18309 (1993).
24. T. C. Grenfell and D. K. Perovich, "Spectral albedos of sea ice and incident solar irradiance in the southern Beaufort Sea," J. Geophys. Res. **89,** 3573–3580 (1984).
25. E. M. Patterson, D. A. Gillette, and B. H. Stockton, "Complex index of refraction between 300 and 700 nm for Saharan aerosols," J. Geophys. Res. **82,** 3153–3160 (1977).
26. S. Gerland, G. E. Liston, J.-G. Winther, J. B. Ørbæk, and B. V. Ivanov, "Attenuation of solar radiation in Arctic snow: field observations and modelling," Ann. Glaciol. **31,** 364–368 (2000).
27. S. G. Warren and A. D. Clarke, "Soot in the atmosphere and snow surface of Antarctica," J. Geophys. Res. **95,** 1811–1816 (1990).
28. C. F. Bohren, "Colors of snow, frozen waterfalls, and icebergs," J. Opt. Soc. Am. **73,** 1646–1652 (1983).
29. P. J. Stephenson, "Some considerations of snow metamorphism in the Antarctic ice sheet in the light of ice crystal studies," in *Physics of Snow and Ice,* H. Oura, ed. (Bunyeido, 1967), pp. 725–740.
30. G. H. Liljequist, "Energy exchange of an Antarctic snowfield: short-wave radiation (Maudheim 71°01′S, 10°65′W)," *Norwegian-British-Swedish Antarctic Expedition, 1949–1952: Scientific Results* (Norsk Polarinstitutt, 1956), Vol. 2(1A).
31. T. C. Grenfell and G. A. Maykut, "The optical properties of ice and snow in the Arctic Basin," J. Glaciol. **18,** 445–463 (1977).
32. S. G. Warren, "Optical properties of snow," Rev. Geophys. Space Phys. **20,** 67–89 (1982).
33. E. R. LaChapelle, *Field Guide to Snow Crystals* (University of Washington Press, 1969).
34. W. J. Wiscombe and S. G. Warren, "A model for the spectral albedo of snow. I: Pure snow," J. Atmos. Sci. **37,** 2712–2733 (1980).
35. D. Beaglehole, B. Ramanathan, and J. Rumberg, "The UV to IR transmittance of Antarctic snow," J. Geophys. Res. **103,** 8849–8857 (1998).
36. S. Bourgeois, "Extinction of solar radiation within snow cover," M. S. thesis (Eidgenössische Technische Hochschule, Zürich, Switzerland, 2002).
37. E. Raschke and A. Ohmura, "Radiation budget of the climate system," in *Observed Global Climate,* M. Hantel, ed. (Springer, 2005), Chap. 4.
38. W. Haeberli, "Sahara dust in the Alps—a short review," Z. Gletscherkunde Glazialgeol. **13,** 206–208 (1977).
39. M. D. King and W. R. Simpson, "Extinction of UV radiation in Arctic snow at Alert, Canada (82°N)," J. Geophys. Res. **106,** 12499–12507 (2001).
40. M. Kuhn and L. Siogas, "Spectroscopic studies at McMurdo, South Pole and Siple Stations during the austral summer 1977–78," Antarct. J. U.S. **13,** 178–179 (1978).
41. M. Kuhn, University of Innsbruck (personal communication, 1984).
42. R. E. Brandt and S. G. Warren, "Solar heating rates and temperature profiles in Antarctic snow and ice," J. Glaciol. **39,** 99–110 (1993).
43. C. F. Bohren, "Multiple scattering of light and some of its observable consequences," Am. J. Phys. **55,** 524–533 (1987).
44. W. J. Wiscombe, "Improved Mie scattering algorithms," Appl. Opt. **19,** 1505–1509 (1980).
45. T. C. Grenfell, D. K. Perovich, and J. A. Ogren, "Spectral albedos of an alpine snowpack," Cold Regions Sci. Technol. **4,** 121–127 (1981).
46. T. C. Grenfell and S. G. Warren, "Representation of a nonspherical ice particle by a collection of independent spheres for scattering and absorption of radiation," J. Geophys. Res. **104,** 31697–31709 (1999).
47. S. P. Neshyba, T. C. Grenfell, and S. G. Warren, "Representation of a nonspherical ice particle by a collection of independent spheres for scattering and absorption of radiation: II. Hexagonal columns and plates," J. Geophys. Res **108D,** 4448, doi: 10.1029/2002JD003302 (2003).
48. T. C. Grenfell, S. P. Neshyba, and S. G. Warren, "Representation of a nonspherical ice particle by a collection of independent spheres for scattering and absorption of radiation: 3. Hollow columns and plates," J. Geophys. Res. **110D,** doi:10.1029/2005JD005811 (2005).
49. C. F. Bohren and D. R. Huffman, *Absorption and Scattering of Light by Small Particles* (Wiley, 1983).
50. B. Light, Applied Physics Laboratory, University of Washington (personal communication, 2006).
51. B. Light, G. A. Maykut, and T. C. Grenfell, "A two-dimensional Monte Carlo model of radiative transfer in sea ice," J. Geophys. Res. **108C,** 3219, doi:10.1029/2002JC001513 (2003).
52. A. Royer, M. DeAngelis, and J. R. Petit, "A 30,000 year record of physical and optical properties of microparticles from an East Antarctic ice core and implications for paleoclimate reconstruction models," Clim. Change **5,** 381–412 (1983).
53. M. Kumai, "Identification of nuclei and concentrations of chemical species in snow crystals sampled at the South Pole," J. Atmos. Sci. **33,** 833–841 (1976).
54. S. G. Warren and W. J. Wiscombe, "A model for the spectral albedo of snow. II: Snow containing atmospheric aerosols," J. Atmos. Sci. **37,** 2734–2745 (1980).
55. A. D. Clarke, K. J. Noone, J. Heintzenberg, S. G. Warren, and D. S. Covert, "Aerosol light absorption measurement techniques: analysis and intercomparisons," Atmos. Environ. **21,** 1455–1465 (1987).

56. T. C. Bond and R. W. Bergstrom, "Light absorption by carbonaceous particles: an investigative review," Aerosol Sci. Technol. **40,** 27–67 (2006).
57. P. Chylek, V. Ramaswamy, and V. Srivastava, "Albedo of soot-contaminated snow," J. Geophys. Res. **88,** 10837–10843 (1983).
58. C. F. Bohren, "Applicability of effective-medium theories to problems of scattering and absorption by nonhomogeneous atmospheric particles," J. Atmos. Sci. **43,** 468–475 (1986).
59. P. B. Price, K. Woschnagg, and D. Chirkin, "Age vs depth of glacial ice at South Pole," Geophys. Res. Lett. **27,** 2129–2132 (2000).
60. R. M. Pope and E. S. Fry, "Absorption spectrum (380–700 nm) of pure water. II. Integrating cavity measurements," Appl. Opt. **36,** 8710–8723 (1997).
61. A. D. Clarke and K. J. Noone, "Soot in the Arctic snowpack: a cause for perturbations in radiative transfer," Atmos. Environ. **19,** 2045–2053 (1985).
62. T. Bond, Department of Civil and Environmental Engineering, University of Illinois (personal communication, 2005).